Fatigue Crack Propagation and Charpy Impact Properties in Armor Steel Welds

ALEKSANDAR CABRILO[1]*, MIROSLAV CVETINOV[2]

[1]Faculty of Technical Sciences, University of Novi Sad, Trg D. Obradovica 6, 21000 Novi Sad, Serbia,

[2] Faculty of Sciences, University of Novi Sad, Trg D. Obradovica 4, 21000 Novi Sad, Serbia

The process of welding armor steel is a complex process because of possible welding faults, appearing in the weld metal zone in the form of cracks and pores. Austenitic filler material is traditionally used for welding armor steels. For heavy structural engineering such as armored military vehicles, which are frequently under the effect of dynamic load, it is important to know the dynamic properties of the most sensitive area of welded joints, the weld metal zone. Due to a significant interest in quantification of material resistance to crack initiation and propagation, the fatigue crack growth rate was measured in the welded metal zone, while the resistance to crack growth in the weld metal was tested by the amount of austenite transformed into martensite. Accordingly, the threshold stress concentration factor was 10 MPa $m^{1/2}$. XRD spectral analysis revealed direct transformation of γ - austenite into α' -martensite.

Key words: Armor steels, Fatigue crack growth, Austenitic stainless steel and Martensitic transformation.

Armor steel belongs to the ultra-high tensile strength and hardness group of steels. The welding of armor steel is complicated due to the high percentage of carbon content in the base metal and the presence of faults in the form of cracks and pores [1] in the weld metal zone, whereby fractures may be initiated in the weld metal. Austenitic filler material is traditionally used for armor steel welding because of hydrogen dilution improved in an austenitic phase [2, 3]. The filler material, in armor steel welded joints has lower mechanical properties than the base material, i.e. the filler material is the weakest point of the welded joint [4]. After the welding process, solidification cracking may result from high thermal expansion of the austenitic stainless steel [5,6] and invisible defects may be created in the weld metal zone [7].

For heavy structural engineering, such as armored military vehicles frequently being under the effects of variable loads [8], mechanical properties of welded joints and the weld metal zone must be known. Due to variable loads, cracks created in the weld metal may easily propagate towards the sensitive fusion line, followed by their possible rapid growth [9].

For armored vehicle structures safe and rational dimensioning, it is necessary to know dynamic effects extreme values and time periods. Therefore, there is a significant interest in material resistance related to crack initiation and propagation, as well as in dynamic force conditions. A fatigue crack growth rate characteristic in the linear and threshold region in metal weld is considered as an important property, since it shows a fault – tolerant ability of this part of welded joint [10,11].

Austenitic filler material is unstable and gets transformed into martensite during fatigue crack propagation due to plastic deformation at the crack tip [12]. During the metastable austenite deformation, two types of martensitic structures can be formed: ε- martensite with hexagonal close packed and α' -martensite, with body centered cubic crystal structure. Austenite into martensite transformation is related to the stacking fault energy. If the stacking fault energy is < 20 J/m^2, transformation proceeds according to the model:$\gamma \rightarrow \varepsilon \rightarrow \alpha$' . If it is larger, then the direct $\gamma \rightarrow \alpha$' transformation occurs [13]. It is known that manganese and nickel stabilize martensite and prevent martensitic transformation. It should be noted that a upper limit of stacking fault energy of austenite-martensite phase transition phase transition varies [14,15]. An amount of austenite transformed into martensite is directly related to crack growth resistance in the weld metal [16].

The main goal of this study was to investigate the impact energy by instrumented pendulum and fatigue crack growth in the Paris region. Martensitic transformation effects on fatigue crack growth in the Paris region were investigated by X – ray diffraction. Fracture surfaces for the impact energy and fatigue crack growth tests were also investigated by Scanning Electron Microscope (SEM). Subsequently, samples in the weld metal region were studied by tensile strength test, hardness measurements, metallography and chemical analysis.

Experimental part

Materials and methods

Materials and welding process

Gas metal arc welding (GMAW) and AWS ER307 solid wire is used for welding armor steel Protac 500. Welding direction is parallel to the rolling direction. Cold rolled plates 12 mm thick are cut to the required dimensions (250 x 100 mm), while V joint under the angle of 55° is prepared by Water Jet Device figure 1. Robot Kuka and Citronix 400A device was used during the welding process testing. Robotic welding is used for human factor effect elimination, in order to allow a fine adjustment of parameters and results repeatability. Wire diameter is 1.0 mm while figure 1 shows V joint dimensions and four - pass welding configuration.

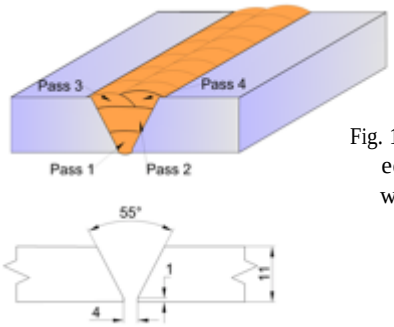

Fig. 1. Schematic drawing of edge preparation and welding configuration

* email: cabrilo@uns.ac.rs

Table 1
CHEMICAL COMPOSITION OF THE BASE MATERIAL

Material	*Chemical composition [wt. %]*											
	C	Si	Mn	S	Cr	P	Al	Cu	Ni	Mo	V	Sn
Protac 500	0.27	1.07	0.71	0.001	0.64	0.009	0.054	0.28	1.09	0.296	0.039	0.011

Table 2
CHEMICAL COMPOSITION OF THE FILLER METAL

Material	*Chemical composition [wt. %]*											
	C	Si	Mn	S	Cr	P	Al	Cu	Ni	Mo	V	Sn
AWS ER307	0.08	0.89	6.29	0.001	17.76	0.014	0.01	0.08	8.24	0.13	0.03	0.011

Base material chemical composition obtained by spectro - chemical analysis is shown in table 1, while the filler material chemical composition is shown in Table 2. Spectro-chemical analysis was performed after the welding process.

As for the fatigue crack growth rate test, it is important to obtain the welded joint without porosity and cracks. Therefore, radiographic testing was being performed after the welding process.

Mechanical property tests

Welded joint tensile strength testing was performed in transverse direction of the weld bead. It should be noted that specimens was cut with Water Jet Device, to eliminate possibilities of thermal effects to high hardness steel. Tensile strength testing was made on servo - hydraulic testing machine Instron 8033. The loading rate was set as 0.125 mm/s until fracture took place. During the tensile test, extensometer was used to monitor and record the stress-strain curves and strain gauge was employed to verify the results obtained by the extensometer.

Metallography testing

The microstructural examination was performed using a Leitz-Orthoplan metallographic microscope and a scanning electron microscope JEOL JSM 6460LV at 25 kV. The samples were ground using SiC papers, polished with a diamond paste and finally etched with a mixture HCl and HNO_3 reagent to reveal the structure.

Fatigue crack growth test

Three point bending specimen, SEN (B) was used for testing [17]. The schematic drawing of specimen for fatigue crack growth test is shown in figure 2. Specimens were cut by Water Jet Device, to eliminate any possibility of armor steel thermal treatment. After getting final measures in the grinding process, 5 mm long machined notch was created on specimens in the direction parallel to welding figure 3, according to the E-647 standard [18]. The fatigue pre-crack was inserted before the crack growth rate tests, in accordance with ASTM E647 [18]. The length of the fatigue pre–crack was 4.7 mm. The fatigue pre-crack was realized with a high-frequency CRACTRONIC pulsator, at a load ratio R = 0.33, followed by a constant loading frequency of 170 Hz. Fatigue crack growth rate was tested on high-frequency CRACTRONIC pulsator, the model with force and frequency control of 145 Hz. The constant sinusoidal shape was used, while the testing was made under the load ratio $R=Kmin/Kmax=0.1$.

During testing procedure, the crack length was measured by RUMUL RMF A-10 measuring foils. In the course of experiments, the number of cycles for each crack growth of 0.05 mm was automatically recorded. On the basis of these records, the diagram of *a-N* was drawn.

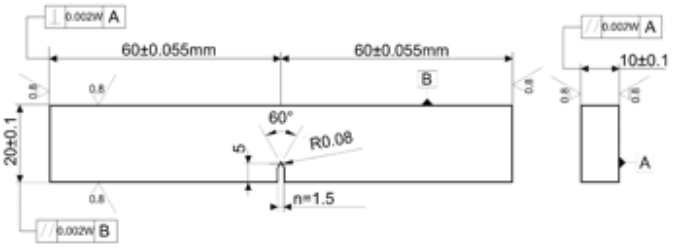

Fig. 2. Schematic drawing of the SEN (B) specimen with dimensions.

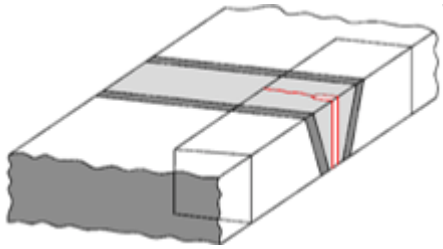

Fig. 3. Specimen orientation with respect to the weld axis for fatigue crack growth test.

a-N curves of dependence were used for crack growth rate *da*/*dN* determination.

The initial dynamic load was determined on the basis of tensile characteristics and maintained during the constant testing period. While the crack was propagating in the number of cycles, the value of ΔK was increasing with the crack length growth.

For this test, three specimens were used, in same testing conditions and initial loads. The result was average value of three measurements. A fracture surface was analyzed by Scanning Electron Microscope JEOL JSM 6460LV at 25 kV.

*Q*uantitative phase analysis by X-ray diffraction

X-ray diffraction was used to identify a martensitic transformation amount formed during the crack propagation, under the effect of fatigue load. Investigation was undertaken by X-ray diffraction in Brag–Brentano θ:2θ reflection geometry, at a room temperature. Diffractograms were recorded on a Philips X-ray diffractometer having a copper tube PW 1830 generator, a PW 1820 goniometer fitted with a post-diffracted graphite monochromator and a scintillation detector attached to a PW 1710 controller (30 kV, 30 mA generator settings, CuKα radiation). LaB_6 was used as an external standard for peak position calibration and for instrumental peak broadening assessment. XRD data were collected over the 2θ range of 40 to 60°, with a step size of 0.05° and an exposition time of 2 s per step.

Martensite to austenite ratio was measured on the fracture surface. After the analysis, the 0.05 mm. Thick

layer was removed, upon which the measurement procedure of austenitic transformation amount was repeated. The repeatability continued to 25% of the austenitic transformation value in martensite. An experimental XRD patterns decomposition (profile fitting) was performed using pseudo - Voigt function on each diffraction peak and linear function on background radiation. For quantitative phase analysis RIR method was employed [19]. The RIR method scales all diffraction data to the standard. By convention, corundum is used as an international reference. The scale factor, I/I_c, was experimentally determined from the pattern strongest line ratio, I, to the corundum I_c strongest line intensity, in a 50/50 weight mixture.

As to determination of martensite and austenite phases weight contents, their scaling factors were obtained from the ICDD PDF-2 database (PDF 41293, PDF 441292, PDF 897245 and PDF 330397). Due to the heavy peak overlapping in the 43° - 44.5° 2θ region, this method could only be employed on the second most intense peak of both martensite, I_{2mart}, and austenite, I_{2aust}, at ~45.0° 2θ [20] and ~50.7° 2θ[21,22], respectively. Intensity ratios of the two strongest lines for martensite, $(I/I_2)_{mart}$, and austenite phase, $(I/I_2)_{aust}$, were thus obtained from the same database. The following equation served for calculation to be done:

$$X_{mart} \cdot I_{2aust} \cdot (I/I_2)_{aust} \cdot (I/I_c)_{mart} = X_{aust} \cdot I_{2mart} \cdot (I/I_2)_{mart} \cdot (I/I_c)_{aust}$$

where $X_{aust} = 1\text{-}X_{mart}$ and X_{mart} are weight fractions of austenite and martensite phases, respectively.

Results and discussions

Radio-graphical results show no visible cracks and porosity in the welded joint, which, according to EN ISO 5817:2014 [23] standard, was B class rated.

Tensile testing results

While tensile characteristics were being tested, a fracture appeared in the weld metal. The tensile strength was 833 MPa, while the yield strength of 552 MPa was within the expected limits figure 4. The difference between tensile and yield strength was 311 MPa, indicating a high ductility of the weld. Toughness was calculated from the area underneath the curve, and was 89 Jm^{-3}.

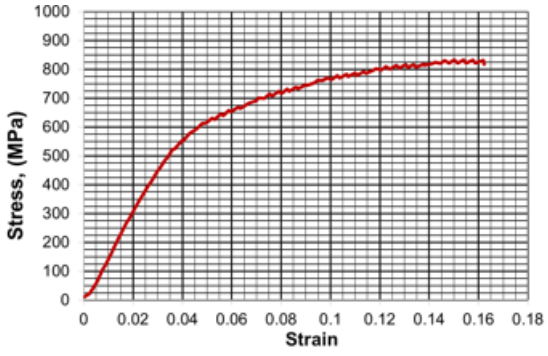

Fig. 4. Stress–strain curve obtained from the base and weld metals transverse tensile testing

Microstructure results

The weld metal micrograph figure 5a consist of austenite with delta ferrite. Delta ferrite becomes finer at lower heat input and cooling rate. In figure 5a, the uniformly distributed morphology of delta ferrite can be seen.

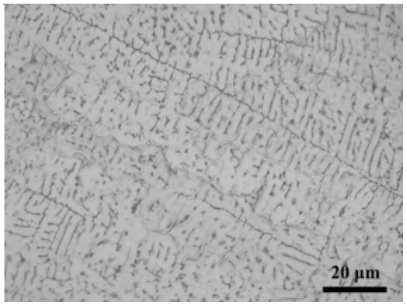

Fig. 5. a) Optical micrograph of AWS ER 307 filler.

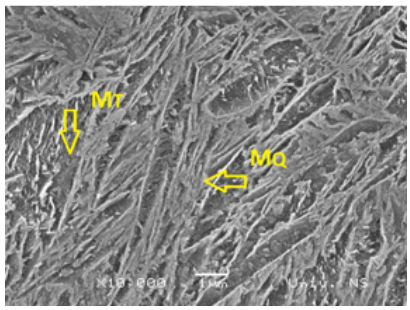

Fig. 5. b) SEM micrograph of base material. M_T - tempered martensite, M_Q - quenched martensite.

Fatigue crack growth behavior

Figure 6 shows the crack growth rate in threshold region $da/dN < 10^{-4}$ mm/cycle. The threshold of stress concentration factor ΔKth is 10 MPa m$^{1/2}$. The residual hydrogen content had no influence on the value of threshold stress concentration factor because of a small amount shown in table 3.

The crack growth rate in the region of linear growth $da/dN > 10^{-4}$ mm/cycle was shown in figure 7. The constants C and m in this region amount to $4x10^{-11}$ and 5.3, respectively. The crack growth seen at the macro level is wavy and tortuous, (fig. 8).

Figure 9 a,b. show the fractograph in the crack growth threshold region in the weld metal zone. The fatigue striations are clearly visible on the fracture surface at at 1 mm from the fatigue crack starting point and their size is about 3 µm.

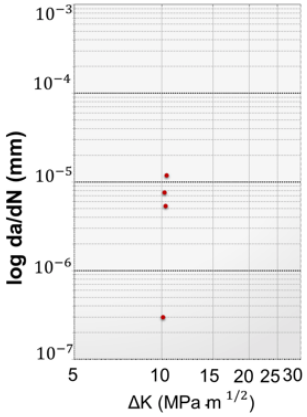

Fig. 6. Fatigue crack growth rate per cycle, da/dN, vs. stress intensity factor range, ΔK, in the near threshold region. Specimens pre-cracked in weld metal, tested at room temperature

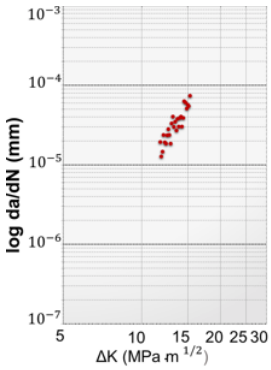

Fig. 7. Fatigue crack growth rate per cycle, da/dN, vs. stress intensity factor range, ΔK, in the linear region.

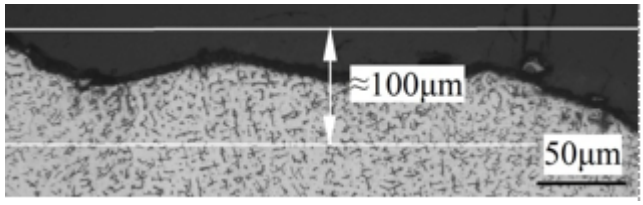

Fig. 8. Fatigue crack growth path in weld metal zone R=0.1. Crack growth direction is from left to right.

	ά - Martensite volume fractions						
Specimen thickness	[mm]	2.50	2.45	2.4	2.35	2.30	2.25
ά -Martensite volume	[%]	55	50	46	34	30	24
Tolerance	[%]	±3	±3	±2	±2	±2	±2

Table 3
α'- MARTENSITE VOLUME FRACTIONS VS. SPECIMEN THICKNESS

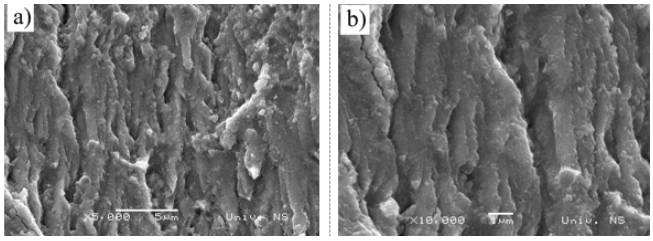

Fig. 9. SEM fractography at 1 mm from the fatigue crack starting point.

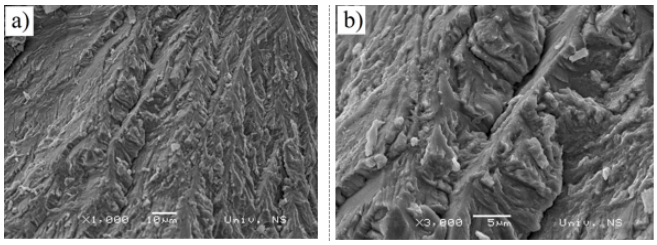

Fig. 10. SEM fractography at 6.5 mm from the fatigue crack starting point.

The fractrograph in the linear crack growth region is shown in figure 10 a and b. The fatigue striations formed in this region are 4 to 5 times larger than in the threshold region, and are up to 15μm large.

XRD spectral analysis

Figure 11 shows the X-ray diffraction results of the deformation-induced α' martensite. The changing amounts are shown per level, in relation to the fracture surface. The results show two phases, austenite and martensite. Both phases have two peaks, austenite with peaks of 2θ from 43.2-43.6 and 50.4-50.9, and martensite with its peaks at 43.5-44.2, 44.8 and 45.0.

Since higher surface roughness causes increased diffuse X-ray scattering, peak intensities inversely correlate with the thickness of the specimens under investigation. Nevertheless, using the RIR method (reference intensity ratio), the ratio of integrated intensities of α' martensite and austenite diffraction peaks reliably indicates their weight ratio in surface layers.

The most intense peaks of α' martensite and austenite overlap not only in our specimen, but in numerous alloys published in crystallographic databases [19]. The uncertainty, inherent in heavily overlapping peaks deconvolution, makes them unsuitable for weight ratio determination. Therefore, the second most intense peaks were used. These peaks are only twice less intense than their stronger counterparts and therefore are absolutely sufficient for precise weight ratio calculation.

Table 3 shows a changes percentage per level in relation to the fracture surface. α'martensite was detected at distances up to 0.25 mm under the fracture surface. The greatest transformation of austenite into α'martensite was 55%, seen on the fracture surface. The amount of α' martensite declines with a distance by an average of H"5%/ 0.05 mm, in the depth perception tests. At the distance of 0.25 mm, the amount of transformed austenite fell to 24%.

Martensitic transformation took place due to plastic deformation at the crack tip. The plastic zone radius, according to Von Mises criterion eq. (1), in the linear growth region, amounts to r^*_{ip} =0.14 mm.

$$r_{1p}^{*} = \frac{1}{4\pi}\left(\frac{K_I}{\sigma_T}\right)^2 \cdot \left(1 + \frac{3}{2}sin^2\theta + \cos\theta\right)\ (mm) \qquad (1)$$

Schram and Reed [24] established a formula for stacking fault energy calculation, an energy affecting a martensitic transformation possibility:

$$SFE = -53 + 6.2(\%Ni) + 0.7(\%Cr) + \\ +3.2(\%Mn) + 9.3(\%Mo)\ (mJm^2) \qquad (2)$$

The stacking fault energy for austenitic filler material is 32 mJ/m^2. This slightly higher stacking fault energy results from the higher manganese and nickel content which exists in austenitic filler material.

It is known that welded joints are very heterogeneous, since they include weld metal, heat affected zone (HAZ) and base metal. Armor steel welded joints are expected to have a tensile strength not lower than 550 MPa, in order to satisfy the requirements of MIL-STD-1185 [25]. The tensile strength achieved in this research of 833 MPa is rather high for austenitic filler material and significantly higher than the tensile strength obtained by other authors [26].

Fatigue induced fracture depends on external factors such as load and internal factors such as mechanical properties of materials and microstructure. It is known that in stainless steel, being metastable materials, austenite transformation into martensite may occur during a fatigue crack growth; this is the result of intensive plastic deformation at the crack tip. X-ray diffraction showed the direct transformation of austenite into α' martensite, what is typical for stainless steel with higher stacking fault energy. Martensitic transformation in these steels causes an increase in volume [27]. The resulting stress and strain fields which appear at the crack tip should be taken into

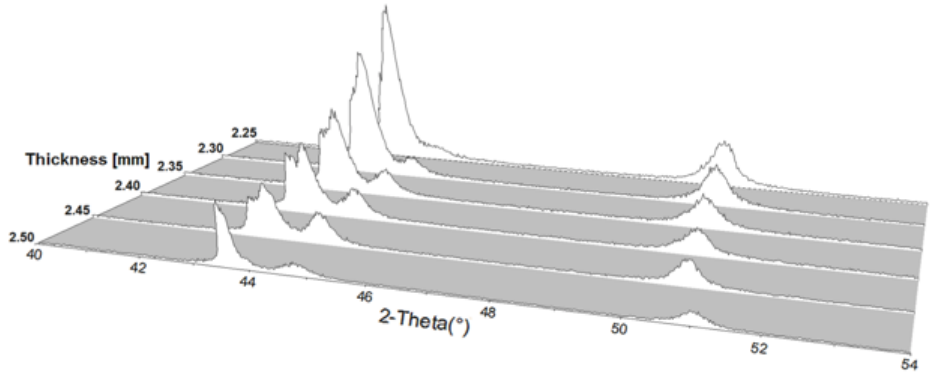

Fig. 11. XRD Diffractograms of specimens under investigation

account during determination of the stress intensity factor [28,29]. Phase transformations taking place at the crack tip [30] decrease the crack growth rate in the linear region [31]. Martensitic transformation takes place only in the thin layer close to the fracture surface. According to eq. (1), the plastic zone in the region of linear growth has a radius of 0.14 mm, which matches the X-ray diffraction results, showing that the zone of intensive martensitic transformation is at a depth of 0.1 mm.

On the basis of transformed martensite percentage, it can be noticed the crack growth is rather difficult. Delta ferrite in the austenitic base of the weld metal gives rise to crack deflection and spreading, thus decreasing the stress intensity factor at the crack tip; it reduces the crack growth rate in this region.

It is known that microstructural characteristics are very important for fatigue crack growth; so, the coefficient defining the crack growth in the Paris region has slightly higher values than usual, which can be explained by the multi - pass weld having an irregular hardened microstructure.

In this research, the crack growth was normally monitored in respect to the growth direction of α'-austenitic dendrite. Regarding to austenitic filler material and cast structure, slightly lower threshold values of stress concentration factor should be expected in the case of cracks growing in the direction parallel to the columnar grain [32].

Conclusions

On the basis of the results presented in this work, the following conclusions may be made:

Tensile strength of weld metal in the specimen welded with austenitic filler metal reached 833 MPa, which is greater than results published for the same filler metal in researches of manual welding.

An effect of the relatively high hardness combined with a high impact energy achieved by using austenitic filler material allows increased resistance to crack initiation with a fatigue crack threshold $\Delta Kth = 10$ MPa $m^{1/2}$, it results in better fatigue performance of the joint. Austenitic filler material showed high threshold stress concentration factor. Microscopic testing showed the rough fracture surface. The crack's growth path is very wavy and tortuous.

Direct transformation of γ- austenite into α'- martensite was ascertained in austenitic filler material AWS 307, with a fault energy of 32 mJ/m^2.

Acknowledgements: The authors would like to thank PhD Zijah Burzic, and Military Technical Institute for Mechanical Testing. This study was financially supported by the Ministry of Education, Science and Technological Development of the Republic of Serbia through the Project Nos. ON 174004. This work was partly supported by the research grant no. OI171015 from the Ministry of Education, Science and Technological Development of the Republic of Serbia.

References

1.ATABAKI, M.M., MA, J., YANG, G., KOVACEVIC, R., Hybrid laser/arc welding of advanced high strength steel in different butt joint configurations, Mater. Des. 64 (2014) 573–587.

2.KUZMIKOVA, L., NORRISH, J., LI, H., CALLAGHAN, M., Research to establish a systematic approach to safe welding procedure development using austenitic filler material for fabrication of high strength steel. 16th International Conference on the Joining of Materials (2011) 1-13

3. BORDEASU, I., MICU, L. M., MITELEA, I., UTU, I. D., PIRVULESCU, L. D., SIRBU, N. A., Cavitation Erosion of HVOF Metal-ceramic Composite Coatings Deposited onto Duplex Stainless Steel Substrate, Mat. Plast.,**53**, no. 4, 2016, p**.** 781

4 MAGUDEESWARAN, G., BALASUBRAMANIAN, V., MADHUSUDHAN, R.G., Effect of welding processes and consumables on high cycle fatigue life of high strength, quenched and tempered joints, Mater. Des. 29 (2008) 1821-1827.

5. RANJBARNODEH, E., POURALIAKBAR, H., KOKABI, A. H., Finite Element Simulation of Carbide Precipitation in Austenitic Stainless Steel 304, Int. J. Mech. Applic. 2 (2012) 117–123.

6. BORDEASU, I.,MITELEA, I., SALCIANU, L., CRACIUNESCU, CM., Cavitation Erosion Mechanisms of Solution Treated X5CrNi18-10 Stainless Steels, JOURNAL OF TRIBOLOGY-TRANSACTIONS OF THE ASME, Volume: 138 Issue: 3, DOI: 10.1115/1.4032489, JUL 2016, Article Number: 031102

7. ALAM, M.M., BARSOUM, Z., JONSEN, P., KAPLAN, A.F.H., HAGGBLAD, H.Å., Influence of defects on fatigue crack propagation in laser hybrid welded eccentric fillet joint, Eng. Fract. Mech. 78 (2011) 2246–2258.

8. CIMPOERU, S.J., The Measurement of Dynamic Structural Stresses in a Light Armoured Vehicle. M.Eng.Sci, GradieAust, In 5 th Australian Aeronautica Conference, Melbourne (1993) 13-15.

9. SHAH KHAN, M.Z., ALKEMADE, S.J., WESTON, G.M., WIESE, D.G., Variable-amplitude fatigue testing of a high hardness armour steel. Int. J. Fatigue Vol.20, No.3 (1998) 233-239.

10. MARTELO, D.F., MATEO, A.M., CHAPETTI M.D., Fatigue crack growth of a metastable austenitic stainless steel, Int. J. Fatigue 80 (2015) 406–416.

11. SHANG, Y.B, SHI, H.J., WANG, Z.X., ZHANG, G.D., In-situ SEM study of short fatigue crack propagation behavior in a dissimilar metal welded joint of nuclear power plant, Mater. Des. 88 (2015) 598–609.

12. MARTELO, D.F., MATEO, A., CHAPETTI, M. D., Crack closure and fatigue crack growth near threshold of a metastable austenitic stainless steel, Int. J. Fatigue 77 (2015) 64–77.

13. MOALLEMI, M., KERMANPUR, A., NAJAFIZADEH, A., REZAEE, A., BAGHBADORANI, S.H., NEZHADFAR, D.P., Deformation-induced martensitic transformation in a 201 austenitic steel. The synergy of stacking fault energy and chemical driving force, Mater.Sci. Eng. A 653 (2016) 147–152.

14. ALLAIN, S., CHATEAU, J.P., BOUAZIZ, O., MIGOT, S., GUELTON, N., Correlations between the calculated stacking fault energy and the plasticity mechanisms in Fe–Mn–C alloys, Mater. Sci. Eng. 387–389 (2004) 158–62.

15. REMY, L., PINEAU, A., Twinning and strain-induced FCC'!HCP transformation in the Fe–Mn–Cr–C system, Mater. Sci. Eng. 28 (1977) 99–107.

16. MEI, Z., MORRIS, J.W., Influence of deformation-induced martensite on fatigue crack propagation in 304-type steels, Metall Trans A 21 (12) (1990) 3137–52.

17.MONAZZAH, A. H., POURALIAKBAR, H., BAGHERI, R., REIHANI S. M. S., Toughness behavior in roll-bonded laminates based on AA6061/SiCp composites, Mater.Sci. Eng. A 598 (2014) 162–173.

18. ***ASTM E647-08: Standard test method for measurement of fatigue crack growth rates. In Annual Book of ASTM Standards, Volume 03.01, West Conshohocken (PA): ASM International; 2004

19. SNYDER, R.L., The Use of Reference Intensity Ratios in X-Ray Quantitative Analysis, Powder Diffraction, **7,** (1992), 186-193.

20. ***ICDD, PDF-2 (Database), #44-1293, International Centre for Diffraction Data, Newtown Square, PA, USA., (2003).

21. ARBUZOV, M., GOLUB, S.Y., KARPETS, M., Structure of austenite ordering in chromium steels, FizikaMetallov i Metallovedenie, 62 (1986) 108-111.

22. AMAR. K.D., DAVID, C., MURDOCK, C.M., SPEER, J.G., MATLOCK, K.D., Quantitative measurement of deformation-induced martensite in 304 stainless steel by X-ray diffraction, Scr. Mater. 50 (2004) 1445-1449.

23.*** EN ISO 5817:2014.Welding. Fusion-welded joints in steel, nickel, titanium and their alloys (beam welding excluded). Quality levels for imperfections.

24. SCHARAM, R.E., REED, R.P., Stacking fault energies of austenitic stainless steels, Metall Trans A (1975) 6A:1345–51.

25. ***MIL-STD-1185. Department of defense manufacturing process standard: welding, high hardness armor; 2008 [SUPERSEDES MIL-W-62162].
26. MAGUDEESWARAN, G., BALASUBRAMANIAN, V.R., Effect of welding processes and consumables on fatigue crack growth behaviour of armour grade quenched and tempered steel joints, Def. Technol. 10 (2014) 47-59.
27.HAUSILD, P., DAVYDOV, V., DRAHOKOUPIL, J., LANDA, M., PILVIN, P., Characterization of strain-induced martensitic transformation in a metastable austenitic stainless steel, Mater. Des. 31 (2010) 1821–1827
28. MITELEA, I; BORDEASU, I; HADAR, A.,The effect of nikel from stainless steels with 13% chromium and 0.10% carbon on the resistance of erosion by cavitation, Rev. Chim. (Bucharest), **56**, no. 11, 2006, p**.** 1169
29. XIONG, F., LIU, Y., Effect of stress-induced martensitic transformation on the crack tip stress-intensity factor in Ni–Mn–Ga shape memory alloy, Acta Mater. 55 (2007) 5621–5629.
30. NAKAJIMA, M., AKITA, M., UEMATSUC Y., TOKAJI, K., Effect of strain-induced martensitic transformation on fatigue behavior of type 304 stainless steel, Procedia Eng. 2 (2010) 323–330.
31. GRUJICIC, M., LAI, S.G., GUMBSCH, P., Atomistic simulation study of the effect of martensitic transformation volume change on crack-tip material evolution and fracture toughness, Mater. Sci. Eng. A231 (1997) 151–162.
32. SHANG, Y.B., SHI, H.J., WANG, Z.X., ZHANG, G.D., In-situ SEM study of short fatigue crack propagation behavior in a dissimilar metal welded joint of nuclear power plant, Mater. Des. 88 (2015) 598–609.

Manuscript received: 15.07.2017